Khulna University Studies Special Issue ICSTEM4IR: 610-624, 2022

ORIGINAL ARTICLE **SCIENCE & ENGINEERING**

HEAT AND MASS TRANSFER SIMULATION OF MHD RADIATIVE CONVECTIVE FLOW OF NANOFLUID THROUGH AN INCLINED POROUS SURFACE

Md. Mehedi Hasan Rasel, Sk. Reza-E-Rabbi*, Sarder Firoz Ahmmed

Mathematics Discipline, Khulna University, Khulna- 9208, Bangladesh

KUS: ICSTEM4IR-22/0116

Manuscript submitted: August 11, 2022 Accepted: September 27, 2022

Abstract

The heat and mass transfer simulation of magnetohydrodynamics (MHD) radiative convective flow of nanofluid through an inclined porous surface are studied. The governing system of couple partial differential equations are transformed into a system of ordinary differential equations. This transformation is done by similarity transformation technique. The numerical solutions are done by sixth order Runge-Kutta method along with Nachtsheim-Swigert shooting iteration technique and then displayed graphically by using Tecplot 9.0. The physical insight of velocity, temperature and concentration have been studied for various physical parameters through numerical calculation and their respective graphs are displayed. Skin friction, rate of heat transfer and rate of mass transfer are also studied for different parameter. Finally, the results are presented in detail with the help of graphs and tables to observe the effect of different parameters like Magnetic parameter (M), radiation parameter (R), thermal Grashof number (Gr), mass Grashof number (Gc), Prandtl number (Pr), Eckert number (Ec) and chemical reaction parameter (Kr).

Keywords: Magnetohydrodynamics, convective flow, nanofluid, porous surface.

Introduction

Magnetohydrodynamics (MHD) plays a significant role in engineering, astrophysics, planetary, plasma physics etc. Magnetic fluids have various effect on many natural and man-made flows. They are vastly used in industry. The terrestrial magnetic field and solar magnetic field, which actually forms the solar flare and sunspots and interplanetary magnetic field carried out by the solar wind. Formally the study of these types of flow is the magnetohydrodynamics. In short, we can define magnetohydrodynamics as, the study of electrically conducting fluids under the effect of magnetic fluids. Examples of magnetofluids are liquid metals, electrolytes, mixture of salt and water, plasmas. In 1970, Hannes Alfven was the first initiator of the field MHD.

*Corresponding author: <rabbi06@math.ku.ac.bd>
DOI: https://doi.org/10.53808/KUS.2022.ICSTEM4IR.0116-se

In recent years, the dynamics of laminar type flow in a porous pipe or channel which expands and contracts received much significance to the researcher. There are different applications of such type of flow in technologies and also in biological flow. Srinivas *et al.* (2016) analytically showed the dynamics of MHD flow of a nanofluid in case of porous pipe with expanding and contracting walls. They analyzed the problems by HAM (Homotopy Analysis Method) and they showed the effect of different parameters. Hayat *et al.* (2015) proposed the MHD flow with the chemical reaction and the effect of power law velocity. HAM (Homotopy Analysis Method) has been used for analytical approach. The combined effect of Hall current and chemical reaction on MHD flow in porous medium has been reported by Rajput and Kanaujia (2016). The solution was carried out by using Laplace transform method. The unstable MHD of nanofluid with varying properties over a stretching plane with heat radiation and chemical response was discussed by Mjankwi, M.A. *et al.* (2019). They employed the fourth order Runge-Kutta method including shooting methodology to conduct their inquiry. Shear stress factor, heat exchange rate and mass exchange rate all decrease as the porosity parameter and magnetic force field increases.

Qureshi *et al.* (2016) discussed the heat and mass transfer of MHD nanofluid in spherical Au-metallic particles. In their paper, a dimensionless Brinkman number was introduced in order to scrutinize variation of the effect of the thermal radiation. They applied similarity transformation method in order to reduce the PDE into nonlinear ordinary differential equation (ODE). For numerical solution they used shooting technique. They found that radiative effects on temperature and mass concentration are totally opposite and the rate of the heat transfer increases with the spherical Au-Metallic nanoparticles.

The unsteady oscillatory flow with non-evenly distributed wall temperature was reported by Falade *et al.* (2017). They considered that the fluid is under the effect of magnetic field and at the lower plate of the proposed model the velocity slip considered. They found that the skin friction increases with the increase of injection on the heated plate. Being motivated by the importance on MHD on nanofluid flow in the different sectors and from above discussion and studies, the present study aims to investigate the heat and mass transfer simulation of MHD radiative convective flow of a nanofluid through inclined porous medium.

Barik *et al.* (2018) reported the MHD flow of visco-elastic fluid through a porous medium. They discussed for the particular cases, the non-conducting and viscous flow. They found that the elasticity properties of the fluid reduce the skin friction at the plate in the presence of porous medium and suction. Recently, Gopal *et al.* (2020) investigated the effect of the higher order chemical reaction on MHD. The solutions were found using Runge-Kutta Fehlberg method. In this research work, the effect of different parameters like Hartmann, Prandtl, Schmidt and Eckert were investigated as well as the effect of these parameters on the chemical reaction. The effect of Hartmann, Prandtl, Schmidt and Eckert were explained vastly. The MHD forced convective flow of finite depth through porous medium in presence of viscous dissipation and also joule heating was proposed by Raju *et al.* (2014). In this research work, they solved the governing equations in the closed form and exact solutions were obtained for velocity distribution as well as temperature distribution. The expressions for different variables were obtained here and the results were presented graphically.

Singh and Alphonsa (2012) reported the oscillatory free convective flow through porous medium in a vertical rotating porous channel. For small and large rotations, the resultant velocities and phase difference on various parameters were discussed in their research work. Ishak *et al.* (2009) analyzed the heat transfer over an unsteady stretching permeable surface with prescribed wall temperature. Keller box method was used to analyze the problem. Effects of the unsteadiness parameter, Prandtl number, suction/injection parameter were examined thoroughly.

Ramana Reddy, G.V. *et al.* (2010) analyzed the mass transfer and radiation effects of unsteady MHD free convective fluid flow embedded in porous medium with heat generation/ absorption. Galerkin finite element method was used to solve the governing equations. The results were discussed for cooling as well as

for heating of the plate. They found that thermal and mass levels decrease with the increase of Prandtl and Schmidt numbers.

Motivated by the above investigations, the mass and heat transit scheme of magnetohydrodynamics radiative convective movement of nanofluid through an inclined permeable surface is presented. The governing model equations are transfigured into ODE with the aid of appropriate similarity transformation. Numerical solutions are done by sixth order Runge-Kutta method in company with Nachtsheim-Swigert shooting reiteration technique. Using visual studio with FORTRAN algorithm. Data are found for varying parameters. Tecplot 9.0 is used to look for graphs. The impacts of dimensionless parameters on dimensionless fluid flow, heat and mass transmission along with heat exchange rate and mass exchange rate are discussed in this research work. The goal is to investigate velocity, heat transfer and mass transfer of nanofluid for inclined porous surface for different parameters.

Materials and Methods

Envision an unstable two-dimensional incompressible magnetohydrodynamics convective flux of a viscous nanofluid across a slanted pervious surface. It is supposed that the impact of different densities with mass transmission and heat transmission take place only on the body force. Therefore, the buoyancy force is induced by the changes in both mass transmission and heat transmission. An analogous chemical reaction of first order accompanied by thermal radiation is taken into account in the stream. An invariable magnetic field is administered at right angles to the plane. Dufour parameter in addition to Soret parameter effect are not in consideration. The flux is also supposed to be in the force's direction. $v_w(t)$ be the mass transfer which is vertical to the surface. Moreover, the surface or wall temperature and concentration are considered as $T_w(x,t)$ and $C_w(x,t)$ respectively and invariable temperature and mass outside the boundary layer are T_∞ and C_∞ .

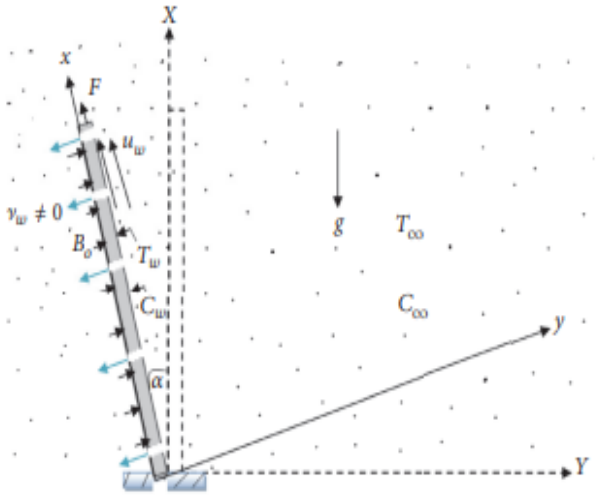

Figure 1. Flow near the inclined sheet. (Mjankwi et al. (2019)).

With the preceding considerations alongside with the Boussineq's boundary layer approximations, the model that governs the continuity equation, momentum equation, energy equation, concentration equation and boundary conditions are provided by the Equations (1) to (5) as,

$$\frac{\partial u}{\partial x}+\frac{\partial v}{\partial y}=0 \tag{1}$$

$$\frac{\partial u}{\partial t}+u\frac{\partial u}{\partial x}+v\frac{\partial v}{\partial y}=\nu^{*}\frac{\partial^2 u}{\partial y^2}-\frac{\nu^{*}}{\kappa^{*}}-\frac{\sigma B_0^2 u}{\rho}+g\beta_T(T-T_\infty)\cos\alpha+g\beta_C(C-C_\infty)\cos\alpha \tag{2}$$

$$\frac{\partial T}{\partial t}+u\frac{\partial T}{\partial x}+v\frac{\partial T}{\partial y}=\frac{1}{\rho c_P}\frac{\partial}{\partial y}\left(K(T)\frac{\partial T}{\partial y}\right)-\frac{1}{\rho c_P}\frac{\partial q_r}{\partial y}+\tau\left\{D_B\left(\frac{\partial C}{\partial y}.\frac{\partial T}{\partial y}\right)+\frac{D_T}{T_\infty}\left(\frac{\partial T}{\partial y}\right)^2\right\}+\frac{\mu}{\rho c_P}\left(\frac{\partial u}{\partial y}\right)^2 \tag{3}$$

$$\frac{\partial C}{\partial t}+u\frac{\partial C}{\partial x}+v\frac{\partial C}{\partial y}=\frac{\partial}{\partial y}\left(D(T)\frac{\partial C}{\partial y}\right)+D_B\frac{\partial^2 C}{\partial y^2}-k_C(C-C_\infty)+\frac{D_T}{T_\infty}\left(\frac{\partial T}{\partial y}\right)^2 \tag{4}$$

At $y=0,\ u=u_w(x,t), v=v_w(x,t),\ T=T_w(x,t),\ C=C_w(x,t)$

As $y\to\infty,\ u\to 0,\ T\to T_\infty,\ C\to C_\infty$ (5)

where t represents the time, ρ be the fluid density, ν^{*} is the kinematic viscosity, K be the conductivity of heat, D be the molecular diffusivity at uniform pressure, u and v are the components of velocity in the x and y direction respectively, the heat capacity is represented as C_p, C is the concentration, μ be the viscous coefficient, κ^{*} is the permeability, K_C be the chemical reaction rate, β_T be the coefficient of volumetric thermal expansion, β_C volumetric expansion coefficient owing to chemical species, T be the temperature of the species, T_∞ and C_∞ are the heat and mass for encompassing atmosphere respectively, electrical conductivity of a material is defined as σ, magnetic field's strength is interpreted as B_0, g be the gravitational acceleration, heat flux from radiation is depicted by q_r, α be the angle of inclination which is calculated by measuring from the vertical axis to the surface, λ be a fixed value, D_T be the dispersal of heat, the rate of initial stretching is c and D_B be the brownian diffusion.The fluid suction velocity is $v_w=-v_0\sqrt{\nu^{*}c/(1-\lambda t)}$, when $v_0>0$, v_0 narrates the wall mass transfer parameter, when $v_0=0$, it is an impermeability condition and when $v_0<0$ it is injection. The q_r (radiation heat flux) is formulated with the Rosseland's approximation provided in the Equation (6),

$$q_r=-\left(\frac{4\sigma^{*}}{3k_1}\right)\frac{\partial T^4}{\partial y} \tag{6}$$

where, Stefan- Boltzmann constant is represented by σ^{*}, k_1 is the factor of absorption. Using Taylor series approach to expanding T^4 about T_∞ is in the Equation (7),

$$T^4=T_\infty^4+4T_\infty^3(T-T_\infty)+\ldots \tag{7}$$

Apart from first degree of T, the higher order terms are ignored, then the Equation (7) becomes,

$$T^4\approx -3T_\infty^4+4T_\infty^3T \tag{8}$$

Replacing the value of T^4 in the Equation (6),

$$q_r = -\left(\frac{4\sigma^*}{3k_1}\right)\frac{\partial T^4}{\partial y} = -\left(\frac{4\sigma^*}{3k_1}\right)\frac{\partial}{\partial y}\left(-3T_\infty^4 + 4T_\infty^3 T\right) = -\left(\frac{16T_\infty^3\sigma^*}{3k_1}\right)\frac{\partial T}{\partial y} \tag{9}$$

The change in flux of radiative heat as a function of y is expressed in the Equation (10),

$$\frac{\partial q_r}{\partial y} = -\left(\frac{16T_\infty^3\sigma^*}{3k_1}\right)\frac{\partial^2 T}{\partial y^2} \tag{10}$$

Substitution of Equation (10) into the second term which changes Equation (3) into Equation (11),

$$\frac{\partial T}{\partial t} + u\frac{\partial T}{\partial x} + v\frac{\partial T}{\partial y} = \frac{1}{\rho c_P}\frac{\partial}{\partial y}\left(K\frac{\partial T}{\partial y}\right) + \frac{1}{\rho c_P}\left(\frac{16T_\infty^3\sigma^*}{3k_1}\right)\frac{\partial^2 T}{\partial y^2} + \tau\left\{D_B\left(\frac{\partial C}{\partial y}.\frac{\partial T}{\partial y}\right) + \frac{D_T}{T_\infty}\left(\frac{\partial T}{\partial y}\right)^2\right\} + \frac{\mu}{\rho c_P}\left(\frac{\partial u}{\partial y}\right)^2 \tag{11}$$

Consider, the relations given by the Equation (12) are,

$$T(x,t) = T_\infty + \frac{bx}{(1-\lambda t)^2}\theta(\eta);\ C(x,t) = C_\infty + \frac{bx}{(1-\lambda t)^2}\phi(\eta) \tag{12}$$

The conductivity of heat for the nanofluid $K(T)$ and coefficient of diffusion $D(T)$ can vary linearly via functions given in the Equation (13),

$$K(T) = K_\infty(1+\frac{\beta_1}{\Delta T}(T-T_\infty);\ D(T) = D_\infty(1+\frac{\beta_2}{\Delta T}(T-T_\infty) \tag{13}$$

The Equation (13) might alternatively be written with regard to dimensionless temperature and it is then reduced to the Equation (14),

$$K(\theta) = K_\infty(1+\beta_1\theta);\ D(\theta) = D_\infty(1+\beta_2\theta) \tag{14}$$

where $K(\theta)$ be the variant conductivity of heat with regard to temperature of no dimension, in terms of dimensionless temperature, $D(\theta)$ is the variant diffusion coefficient, D_∞ be the coefficient of fluid diffusion at the separation of the sheet, K_∞ be the conductivity of heat at sheet's separation, β_1 relies on the character of the fluid and estimates the thermodynamic conductivity change in the company of temperature and β_2 also relies on the fluid properties and enumerates the rate of change in chemical diffusivity as well as heat.

Applying the similarity transformation to the PDEs (2), (4), (11) and (5) which are then transfigured to a system of couple ODE given in Equation (15),

$$\eta = \sqrt{\frac{c}{\nu^*(1-\lambda t)}}y;\ \psi = \sqrt{\frac{c\nu^*}{(1-\lambda t)}}xf(\eta);\ \theta(\eta) = \frac{T-T_\infty}{T_w-T_\infty};\ \phi(\eta) = \frac{C-C_\infty}{C_w-C_\infty} \tag{15}$$

Stream function is $\psi(x,y)$ in this case and the components of velocity in the direction of axes are given in the Equation (16),

$$u = \frac{\partial\psi}{\partial y} = \left(\frac{cx}{1-\lambda t}\right)f'(\eta);\ v = -\frac{\partial\psi}{\partial x} = -\left(\frac{c\nu^*}{1-\lambda t}\right)f(\eta) \tag{16}$$

The continuity equation is satisfied by the Equation (16), $f(\eta)$ stands for suction together with injection. $\theta(\eta)$ and $\phi(\eta)$ are the heat and concentration of the fluid with no dimension respectively, η be the

space variable with no dimension. Using dimensionless variables and velocity components u and v, transforming the Equations (2), (11) and (4) into the ordinary differential Equations (17) to (18) respectively are obtained as,

$$f''' = A\frac{\eta}{2}f'' + [A + M + \varphi]f' + \left(f'\right)^2 - ff'' - Gr\theta - Gc\phi \tag{17}$$

$$\theta'' = \frac{-\beta_1(\theta')^2 + \Pr[A\frac{\eta}{2}\theta' + 2A\theta + f'\theta - f\theta' - Ec(f'')^2 - Nt\left(\theta'\right)^2 - Nb\theta'\phi']}{1 + R + \beta_1\theta} \tag{18}$$

$$\phi'' = \frac{-\beta_2\phi'\theta' + Sc[A\frac{\eta}{2}\phi' + 2A\phi + f'\phi - f\phi' + Kr\phi - Nt'\theta']}{1 + Db + \beta_2\theta} \tag{19}$$

The dimensionless initial and boundary conditions are stated in the Equation (20),

At $\eta = 0, \quad f(0) = f_w;\ f'(0) = 1;\ \theta(0) = 1;\ \phi(0) = 1$

As $\eta \to \infty \quad f'(\eta) \to 0;\ \theta(\eta) \to 0;\ \phi(\eta) \to 0$ (20)

The non- dimensional parameters are,

Unsteadiness parameter, $A = \frac{\lambda}{c}$, Magnetic parameter, $M = \frac{\sigma B_0^2(1-\lambda t)}{\rho c}$, porosity term, φ, Thermal Grashof number, $Gr = \frac{g\beta_T x(T_W - T_\infty)}{u_W^2}\cos\alpha$, Prandtl number, $\Pr = \frac{C_P\mu}{K_\infty}$, Mass Grashof number $, Gc = \frac{g\beta_C x(C_W - C_\infty)}{u_W^2}\cos\alpha$, Eckert number, $Ec = \frac{u_W^2}{C_P(T_W - T_\infty)}$, Thermophoresis parameter, $Nt = \frac{\tau D_T}{T_\infty \upsilon^*}(T_W - T_\infty)$, Brownian motion parameter, $Nb = \frac{\tau D_B}{\upsilon^*}(C_W - C_\infty)$, Radiation parameter, $R = \frac{16T_\infty^3\sigma^*}{3k_1K_\infty}$, Schmidt number, $Sc = \frac{\upsilon^*}{D_\infty}$, Chemical reaction parameter, $Kr = \frac{K_C(1-\lambda t)}{c}$, $Db = \frac{Sc}{Le}$. The skin friction coefficient or shear stress factor (C_f), the Nusselt number or rate of heat transfer (Nu_x) and the Sherwood number or rate of mass transfer (Sh_x) are specified in the Equation (21),

$$C_f = \frac{\tau_w}{(1/2)\rho u_w^2}\ ;\ Nu_x = \frac{xq_w}{K(T_w - T_\infty)}\ ;\ Sh_x = \frac{xh_m}{D(C_w - C_\infty)} \tag{21}$$

where $\tau_w = \mu\left[\frac{\partial u}{\partial y}\right]_{y=0}\ ;\ q_w = -K\left[\frac{\partial T}{\partial y}\right]_{y=0}\ ;\ h_m = -D\left[\frac{\partial C}{\partial y}\right]_{y=0}$ and τ_w, q_w and h_m are skin friction, heat exchange rate and rate of mass exchange respectively. Substituting the dimensionless variable in Equations (21) is transformed into Equation (22),

$$f''(0) = \frac{1}{2}\sqrt{\mathrm{Re}_x}C_f \; ; \; -\theta'(0) = \frac{Nu_x}{\sqrt{\mathrm{Re}_x}} \; ; \; -\phi'(0) = \frac{Sh_x}{\sqrt{\mathrm{Re}_x}} \tag{22}$$

where, $f''(0)$, $-\theta'(0)$ and $-\phi'(0)$ are the skin friction, Nusselt number and Sherwood number respectively and $\mathrm{Re}_x = {u_w x}/{\nu^*} = {cx^2}/{\nu^*(1-\lambda t)}$ is the local Reynolds number.

Numerical Analysis

Many physical phenomena in applied science and engineering are appears in the non-linear coupled partial differential equations. This system of equations can be solved analytically although it is difficult to solve. An initial value solver, sixth order Runge-Kutta method along with Nachtsheim-Swigert shooting iteration technique have been used in this proposed work. There are three asymptotic boundary condition and hence three unknown surface conditions are $f''(0), \theta'(0)$ and $\phi'(0)$. The outer boundary conditions are given in the Equation (23),

$$\begin{aligned}
f'(\eta_{\max}) &= f'(f''(0), \theta'(0), \phi'(0)) = \delta_1 \\
\theta(\eta_{\max}) &= \theta(f''(0), \theta'(0), \phi'(0)) = \delta_2 \\
\phi(\eta_{\max}) &= \phi(f''(0), \theta'(0), \phi'(0)) = \delta_3 \\
f''(\eta_{\max}) &= f''(f''(0), \theta'(0), \phi'(0)) = \delta_4 \\
\theta'(\eta_{\max}) &= \theta'(f''(0), \theta'(0), \phi'(0)) = \delta_5 \\
\phi'(\eta_{\max}) &= \phi'(f''(0), \theta'(0), \phi'(0)) = \delta_6
\end{aligned} \tag{23}$$

Considering, $f''(0) = g_1, \theta'(0) = g_2, \phi'(0) = g_3$ and the minimum value of the error is given in the error function is given in the Equation (24),

$$E = \delta_1^2 + \delta_2^2 + \delta_3^2 + \delta_4^2 + \delta_5^2 + \delta_6^2 \tag{24}$$

In order to get the solutions as an initial value problem, we need a value for $f''(0), \theta'(0)$ and $\phi'(0)$. The most important factor of shooting method is to find the appropriate finite values of η_∞ . In order to determine η_∞ , starting with some initial guess value for some particular set of physical parameters to obtain $f''(0)$ and $\theta'(0)$. The technique is repeated with a larger value of η_∞ until the difference between successive values of $f''(0)$ and $\theta'(0)$ is only significant digit. The choosen last value of η_∞ is the most appropriate value for η_∞ for particular set of parameters. This may change for another set of pertinent parameters. The process is completed once the finite value of η_∞ has been determined. After each iteration, it is required to satisfy the boundary conditions and in order to get a better approximation for the solution to adjust the approximated values.

Large values cause the trial integration to diverge or the surface boundary conditions to slowly converge. In terms of computer time, selecting too large values is costly. Nachtsheim-Swigert devised an iteration method for dealing with dealing with these problems. In order to get the solution Runge-kutta sixth order method with Nachtsheim-Swigert shooting iteration technique has been used with step size h=0.01. The process repeated until the desired accuracy of degree 10^{-4} is obtained.

Results and Discussion

Nanofluid flow through an inclined permeable surface with hydromagnetic radiative convective properties has been investigated numerically. This section describes different physical elements that have been emerged in the mathematical formulation. The results have been discussed in the previous section in order to determine the physical behaviour of the proposed problem are presented through graphs from Figure 2 to Figure 19. Validation of result of the problem is given in the Table 1,

Table 1. Comparison of Pr, β_1 and β_2 for temperature and rate of heat transfer.

Increasing of the flow parameter	Temper-ature (Mjankwi etal. (2019))	Rate of heat transfer (Mjankwi et al.(2019))	Temper-ature (Ishak et al. (2009))	Rate of heat transfer (Ishak et al. (2009))	Temper-ature	Rate of heat transfer
Pr	D	I	D	I	D	I
β_1	I	--	--	--	I	I
β_2	I	--	--	--	I	I

where '*D*' and '*I*' represent the decreasing rate and increasing rate respectively. In table 1, it represents the comparison of Pr, β_1 and β_2 for temperature and rate of heat transfer. It can be seen that the present simulation can predict the previous results with an insignificant changes.

The value of the main parameters are considered for Figure 2 to Figure 19 as,

$f_w = 0.1, A = 0.5, \varphi = U = 0.5, M = 0.5, Gr = 0.1, Gc = 0.1, \beta_1 = 0.012, \beta_2 = 0.01, \Pr = 0.72, R = 0.01,$
$Kr = 0.1, Ec = 0.03, Sc = 0.22, Db = 0.2, Nt = 0.5, Nb = 0.4, AI = 1^0$ and $Nt' = 0.3$

The typical consequences of unsteadiness parameter (A) on the profiles of velocity is presented in Figure 2. It is noted that rise in unsteadiness parameter results in the decrease of fluid's velocity. For η=0.4, the velocity for *A=0.5, A=0.6* and *A=0.7* are 0.7577, 0.7536 and 0.7494 respectively. Therefore, velocity decreases with respect to the increase of the value of A. For *A=0.5* to *A=0.6*, the diminution in velocity is 0.0041. The rate of diminution is 4.1%. For *A=0.5* to *A=0.6*, the diminution in velocity is 0.0083. The rate of diminution is 4.15%. There is the thickening of the thermal boundary layer for the increase of unsteadiness parameter. Due to the increase of initial stretching rate, there is a decrease of unsteadiness parameter. Unsteadiness parameter influences the boundary layer and provides retardation in velocity. So, the increase of unsteadiness parameter decreases the velocity.

Figure 3 shows how the magnetic parameter (M) affects the velocity profiles. It is noticed that with the increase of magnetic parameter the velocity decreases. The presence of magnetic fields generates the frictional force or drag force or Lorentz force which opposes and retards the fluid's motion. For η=0.52, the velocities for *M=0.5, M=0.6,* and *M=0.7* are 0.6398, 0.6338 and 0.6278. The decrement for *M=0.5* to *M=0.6* is 0.006. The rate of decrement is 6% and the decrement for *M=0.5* to *M=0.7* is 0.012 and the rate of decrement is 6%. There is an increase of electrical conductivity and magnetic induction in the company of the increase of magnetic parameter. With the increase of density of the nanofluid and initial stretching rate, the magnetic parameter decreases.

DOI: https://doi.org/10.53808/KUS.2022.ICSTEM4IR.0116-se

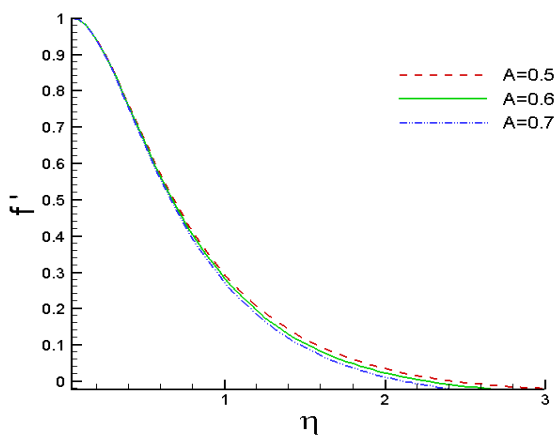

Figure 2. Impacts of various A on the field of velocity.

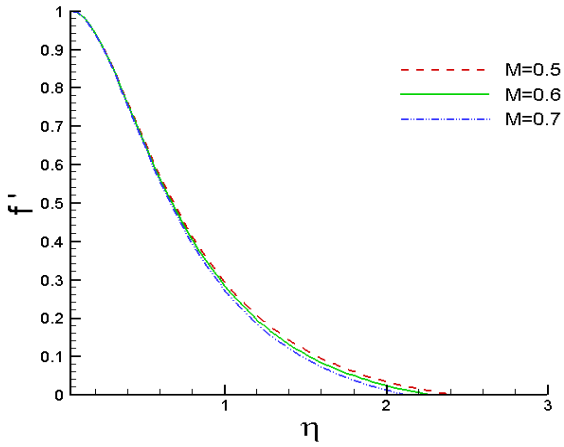

Figure 3. Impacts of various M on the field of velocity.

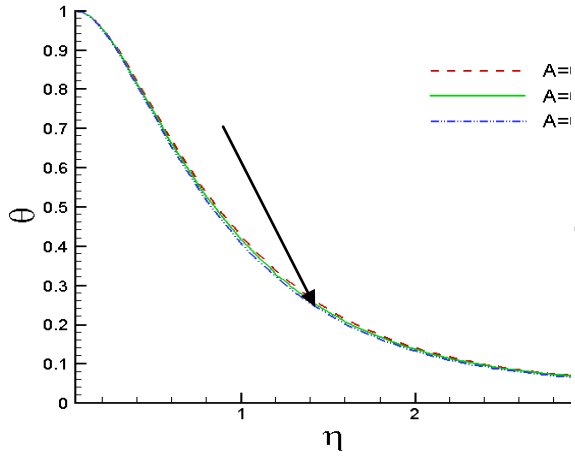

Figure 4. Impacts of various A on the field of temperature.

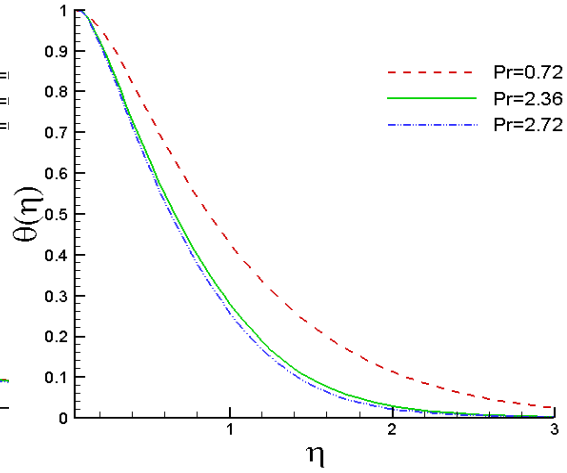

Figure 5. Impacts of various Pr on the field of temperature.

Figure 4 represents the typical impacts of unsteadiness parameter (A) on the field of temperature. It has been shown that increasing unsteadiness parameter causes the field of temperature of the nanofluid to decrease. For η=0.4, the temperatures for $A=0.5$, $A=0.6$ and $A=0.7$ are 0.818, 0.8125 and 0.8071 respectively. Therefore, with an increase in the values of the A, the temperature drops. For $A=0.5$ to $A=0.6$, the diminution in temperature is 0.0055. The rate of diminution is 5.5%. For $A=0.5$ to $A=0.7$, the diminution in temperature is 0.0109 and the rate of diminution is 5.4%. Thickness of thermal boundary layer decreases with the increase of A. This causes decrement of the dimensionless temperature. The effects of Prandtl number (Pr)

on the temperature profiles is demonstrated in Figure 5. Temperature decreases with the increase of Prandtl number. The value of the Prandtl number is chosen as *Pr=0.72, Pr =2.36* and *Pr= 2.72* which conforms to air at 30° C, carbon di-sulphide at 25° C and methyl chloride at 30° C. For η=1.0, the temperatures for *Pr=0.72, Pr=2.36* and *Pr=2.72* are 0.4268, 0.2778 and 0.2564. For *Pr=0.72* to *Pr=2.36*, the decrement is 0.149. The rate of decrement is 9.085%.

For *Pr=0.72* to *Pr=2.36*, the decrement is 0.149. The rate of decrement is 9.085%. For *Pr=0.72* to *Pr=2.72*, the diminution is 0.1704 and the rate of diminution is 8.52%.

The impacts of variable thermal conductivity on the temperature profile is revealed in Figure 6. It demonstrates that with the increase of variable thermal conductivity there is an increase in the temperature of nanofluid. It is due to the fact that the increase in the thermal boundary layer thickness. It shows that for η=0.6, for β_1=0.012, β_1=1.012 and β_1=2.012 the fluid temperatures are 0.6675, 0.72482 and 0.7482 respectively. The rate of increment for β_1=0.012 to β_1=1.012 is 5.7% and for β_1=0.012 to β_1=2.012 is 4.035%. Figure 7 represents the effect of variable diffusion coefficient parameter on the temperature profile. It depicts that an increase in variable diffusion coefficient parameter there is an increase in the fluid temperature. For η=0.6, for β_2=0.01, β_2=0.5 and β_2=1.5 the temperatures are 0.6676, 0.6712 and 0.6755 respectively. The rate of increment for β_2=0.01 to β_2=0.5 is 0.73% and for β_2=0.01 to β_2=1.5 is 0.43%. The effects of thermal radiation parameter (*R*) on the temperature profile is displayed in Figure 8. It is noted that with the increase of thermal radiation parameter there is an increase in the temperature of the fluid. In order to boost the heat transfer rate, when the thermal radiation parameter grows, the thickness of the boundary layer increases. For η= 0.4, the temperatures for *R=0.01, R=1.0* and *R=2.0* are 0.8180, 0.8436 and 0.8528 respectively. Therefore, the rate of gain is 2.59% for *R=0.01* to *R=1.0* and for *R=0.01* to *R=2.0* is 0.92%. The effects of the Brownian parameter (*Nb*) on the temperature profile is depicted in Figure 9. It is observed that with the increase of the thermophoresis parameter there is an increase in the flow of nanofluid. For η=0.6, for *Nb=0.4, Nb=1.4* and *Nb=2.4* the temperatures are 0.6675, 0.6905, and 0.71002. The increment is 0.023 for *Nb=0.4* to *Nb=1.4* and the rate of increment is 2.3%.

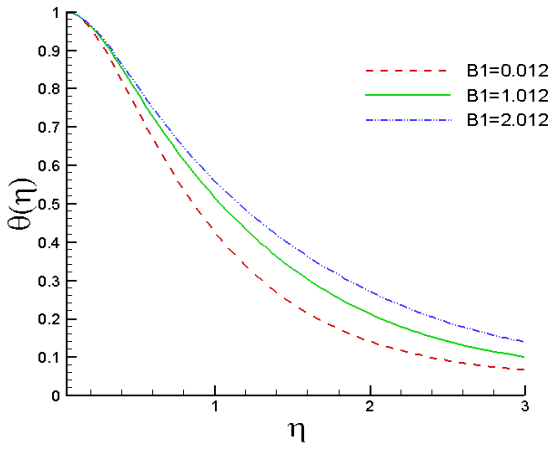

Figure 6. Impacts of variable thermal conductivity on the field of temperature.

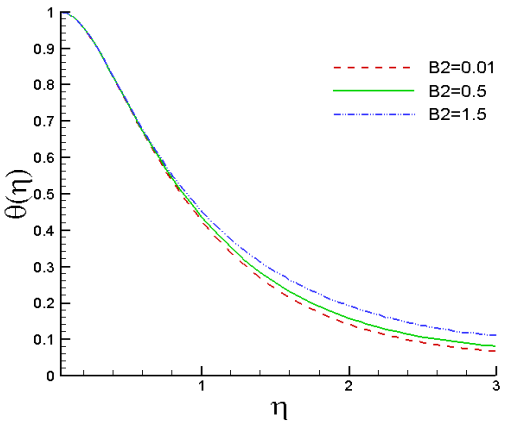

Figure 7. Impacts of variable diffusion coefficient on the field of temperature.

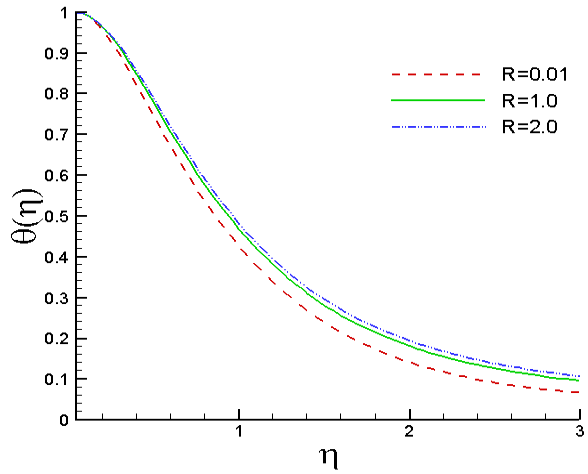

Figure 8. Impacts of various *R* on the field of temperature.

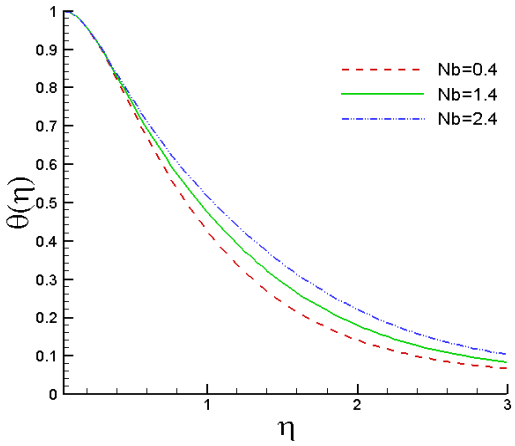

Figure 9. Impacts of various *Nb* on the field of temperature.

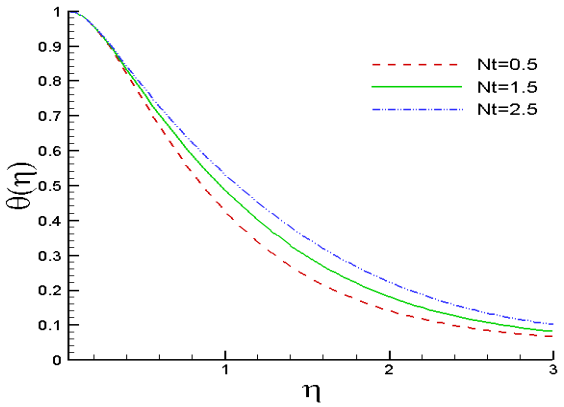

Figure 10. Impacts of various *Nt* on the field of temperature.

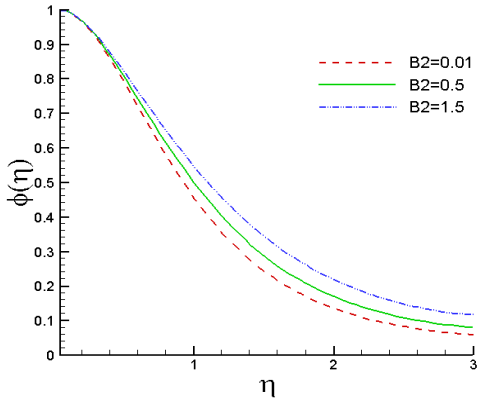

Figure 11. Impacts of variable diffusion coefficient on the field of concentration.

The increment is 0.04252 for *Nb=0.4* to *Nb=2.4* and the rate of increment is 1.96%. The effects of the thermophoresis parameter (*Nt*) on the temperature profile is presented in Figure 10. It is seen that velocity of the fluid increases with the increase of the thermophoresis parameter. For η=0.4, for *Nt=0.5, Nt=1.5* and *Nt=2.5* the temperatures are 0.818, 0.8303 and 0.8404 respectively. The increment is 0.0123 for *Nt=0.5* to *Nt=1.5* and the rate of increment is 0.0224%. The rate increment for *Nt=0.5* to *Nt=2.5* is 1.01%. Figure 11 demonstrates the effects of variable diffusion coefficient parameter (β_2) on the concentration profile. It shows that an increase in variable diffusion coefficient parameter there is an increase in the fluid flow. At 0.6, for β_2=0.01, β_2=0.5 and β_2=1.5 the concentrations are 0.71735, 0.7399 and 0.7622 respectively. The rate of increment for β_2=0.01 to β_2=0.5 is 4.6% and for β_2=0.01 to β_2=1.5 is 2.23%.

The effects of the brownian parameter (*Nb*) on the concentration profile is displayed in Figure 12. It is observed that the mass transport of nanofluids increases as the brownian parameter is increased. For η=0.6,

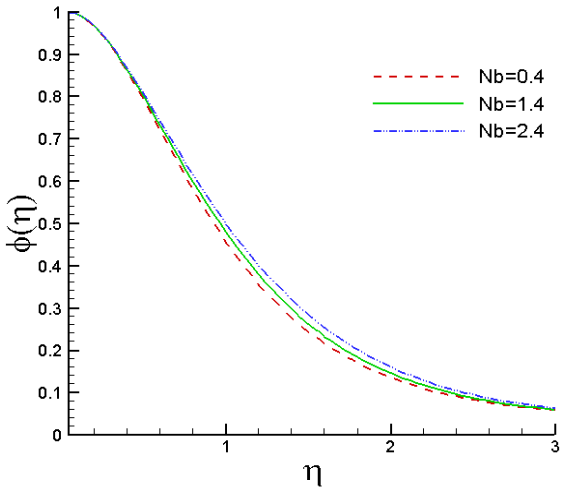

Figure 12. Impacts of various *Nb* on the field of concentration.

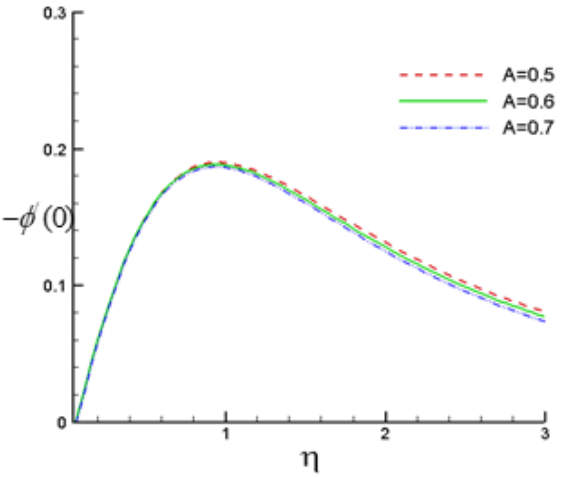

Figure 13. Impacts of various *A* on the rate of mass exchange.

for *Nb=0.4, Nb=1.4* and *Nb=2.4* the concentrations are 0.71735, 0.7291 and 0.7397. The increment is 0.01175 for *Nb=0.4* to *Nb=1.4* and the rate of increment is 1.175%. The increment is 0.02235 for *Nb=0.4* to *Nb=2.4* and the rate of increment is 1.06%. Figure 13 and Figure 14 represent the effect of unsteadiness parameter (*A*) on rate of mass transport (Nu_x) and rate of heat transport (Sh_x) respectively. Rate of mass transfer decreases with the increase of unsteadiness parameter. For η=0.4, for *A=0.5, A=0.6* and *A=0.7* the Sherwood numbers are 0.288, 0.2862 and 0.2844. The rate of decrement for *A=0.5* to *A=0.6* is 1.8% and for *A=0.5* to *A=0.7* is 1.8%. Rate of heat transfer decreases with the increase of unsteadiness parameter. For η=0.4, for *A=0.5, A=0.6* and *A=0.7* the rate of heat transfers are 0.2373, 0.2291 and 0.2210. The rate of decrement for *A=0.5* to *A=0.6* is 8.2% and for *A=0.5* to *A=0.7* is 8.1%.

Figure 15 shows the effects of variable thermal conductivity on rate of heat transfer. Rate of heat transfer increases with the increase of variable thermal conductivity. For η=0.6, the rate of heat transfer for β_1=0.012, β_1=1.012 and β_1=2.012 are 0.2969, 0.3313 and 0.3448 respectively. The rate of increment for β_1=0.012 to β_1=1.012 is 3.44% and for β_1=0.012 to β_1=2.012 is 1.35%.

The effects of variable diffusion coefficient on rate of mass transfer and rate of heat transfer are discussed in Figure 16 and Figure 17 respectively. Rate of mass transfer increases with the increase of variable diffusion coefficient. For η=0.6, for β_2=0.01, β_2=0.5 and β_2=1.5 the Sherwood numbers are 0.3774, 0.3787 and 0.3802. The rate of increment for β_2=0.01 to β_2=0.5 is 0.265% and for β_2=0.01 to β_2=1.5 is 0.15%. Rate of heat transfer increases with the increase of variable thermal conductivity. At 0.6, for β_2=0.01, β_2=0.5, β_2=1.5 the rate of heat transfers are 0.2969, 0.2893 and 0.2803 respectively. The rate of increment for β_2=0.01 to β_2=0.5 is 1.55% and for β_2=0.01 to β_2=1.5 is 1.11%. The impacts of inclination of porous surface for velocity and temperature are depicted in Figure 18 and Figure 19. It represents that the velocity and temperature decreases with the increase of inclination of the porous surface. This is due to the resistance created by the inclination. The more the inclination the less will be the velocity and temperature.

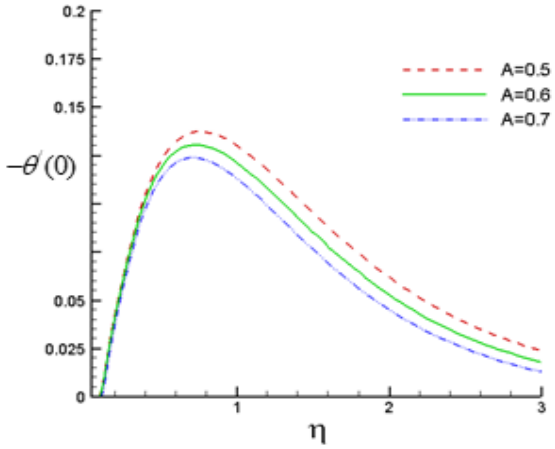

Figure 14. Impacts of various A on the rate of heat exchange.

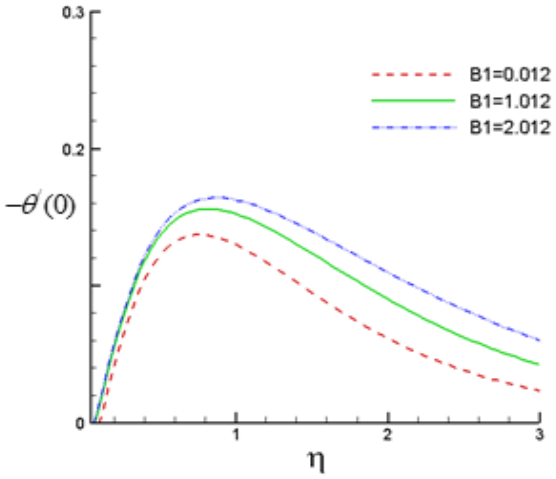

Figure 15. Impacts of various variable thermal conductivity on the rate of heat exchange.

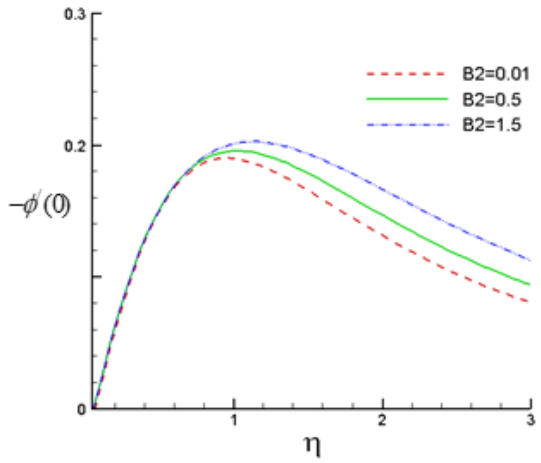

Figure 16. Impacts of variable diffusion coefficient on rate of mass exchange.

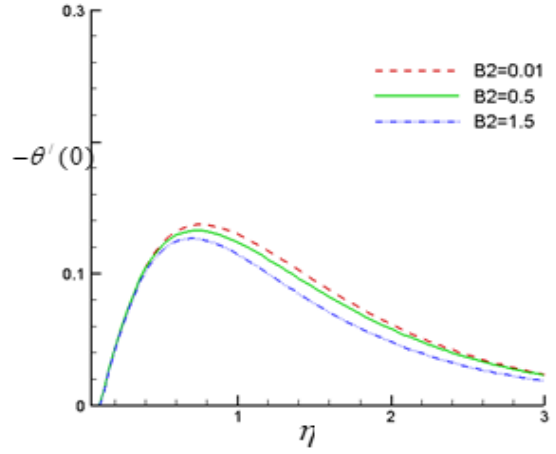

Figure 17. Impacts of variable diffusion coefficient on rate of heat exchange.

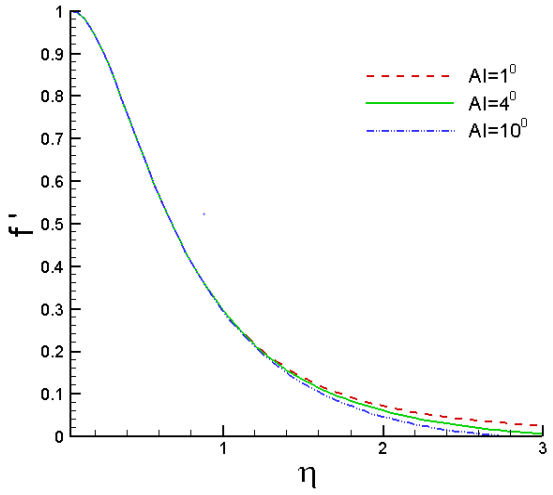

Figure 18. Impacts of inclination of the surface on velocity.

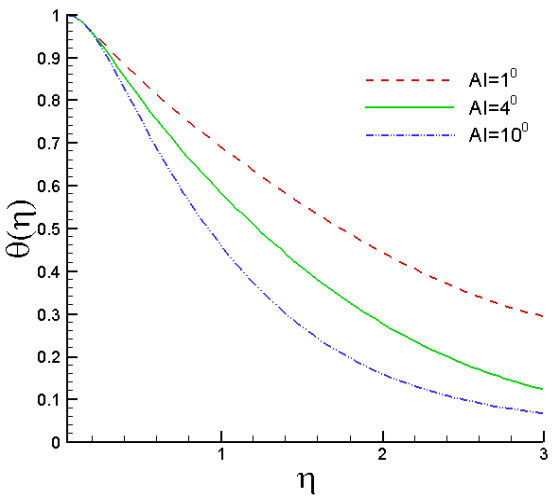

Figure 19. Impacts of inclination of the surafce on temperature.

Conclusion

In this study, a numerical and comparative heat and mass transfer analysis of magnetohydrodynamics (MHD) radiative convective flow of nanofluid through an inclined permeable surface is presented. The effects of the different parameters such as Schmidt number, magnetic parameter, thermal Grashof number, mass Grashof number, unsteadiness parameter, variable thermal conductivity, variable diffusion coefficient, Prandtl number, thermal radiation parameter, chemical reaction parameter, Eckert number, thermophoresis parameter, brownian motion parameter and thermophoresis parameter on the velocity, temperature, concentration as well as skin friction, Nusselt number and Sherwood number has been established.

- An increase in unsteadiness parameter have the tendency to reduce the flow, heat transfer and mass transfer. A rise in variable thermal conductivity enhances the heat transfer but scale down the flow of the fluid and mass transfer.
- With the increase in variable diffusion coefficient there is a decrease in the fluid flow. On the other hand there is an increase in heat and mass transfer.
- There is a rise in the flow and heat transfer for the increase of Eckert number but down in the mass transfer. An increase in mass Grashof number enhances the flow and reduces the heat transfer and mass transfer.
- Flow of the fluid and mass transfer increases with the increase of thermal Grashof number and transfer of heat decreases with the increase of thermal Grashof number.
- A rise in chemical reaction parameter improvises the flow of the fluid but deteriorate the heat and mass transfer. An increase in magnetic parameter enhances heat transfer but reduces the flow and mass transfer.
- The flow of fluid decreases and heat and mass transfer increases with the increase of Brownian parameter. The flow of the fluid and mass deteriorates and heat transfer increases with the increase of thermophoresis parameter.

- A rise in Prandtl number improvises the flow and mass transfer and reduces the heat transfer. Heat transit increases and mass and the fluid flow decreases with the increase of thermal radiation parameter. Flow of the fluid increases and heat and mass transfer decreases with the increase of Schmidt number.

References

Barik, R. N., Dash,G. C., Rath, P. K. (2018). Steady laminar MHD flow of visco-elastic fluid through a porous pipe embedded in a porous medium, *Alexandria Engineering Journal,* 57:973–982.

Falade, J. A., Ukaegbu, J. C., Egere, A. C., Adesanya, S.O. (2017). MHD oscillatory flow through a porous channel saturated with porous medium, *Alexandria Engineering Journal*, 56:147–152.

Gopal, D., Saleem, S., Jagadha, S., Ahmad, F., Almatroud, A. O., Kishan, A. (2020). Numerical analysis of higher order chemical reaction on electrically MHD nanofluid under influence of viscous dissipation, *Alexandria Engineering Journal*, 30:30.

Hayat, T., Rashid, M., Imtiaz, M., Alsaedi, A. (2015). Magnetohydrodynamic (MHD) stretched flow of nanofluid with power-law Velocity and chemical reaction, *AIP Advances, 5*:117121.

Ishak, A., Nazar, R., Pop, I. (2009). Heat transfer over an unsteady stretching permeable surface with prescribed wall temperature. *Nonlinear Analysis: Real World Applications*, 10: 2909-2913.

Mjankwi, M. A., Masanja, V. G., Mureithi, E. W., James, M. N. (2019). Unsteady MHD Flow of Nanofluid with Variable Properties over a Stretching Sheet in the Presence of Thermal Radiation and Chemical Reaction, *International Journal of Mathematics and Mathematical Sciences*, 2019:1-14.

Qureshi,M. Z. A., Rubbab,Q., Irshad,S., Ahmad,S., Aqeel,M. (2016). Heat and MassbTransfer Analysis of MHD Nanofluid Flow with Radiative Heat Effects in the Presence of Spherical Au-Metallic Nanoparticles, *Nanoscale Research Letters,* 11:472.

Rajput, U. S., Kanaujia, N. (2016). Combined effect of Hall current and chemical reaction on MHD flow through Porous medium with heat generation past an impulsively started vertical plate with constant wall temperature and mass diffusion, *Journal of Computational and Applied Research in Mechanical Engineering*, 9(1):117-128.

Raju, K. V. S., Reddy,T. S., Raju, M. C., Narayana, P. V. S., Venkataramana, S. (2014). MHD convective flow through porous medium in a horizontal channel with insulated and impermeable bottom wall in the presence of viscous dissipation and Joule heating, *Ain Shams Engineering Journal,* 5:543–551.

Raman Reddy, G.V., Ramana Murthy, Ch.V., Bhaskar Reddy, N. (2010). Mass transfer and radiation effects of unsteady MHD free convective fluid embedded in porous medium with heat generation/absorption. *Indian Journal of Pure and Applied Physics*, 48: 157-165.

Singh, K. D., Mathew, A. (2012). Free Convective Flow Through Porous Medium in a Rotating Vertical Porous Channel*, Global Journal of Science Frontier Research Mathematics & Decision Sciences,* 12(3): 51-64.

Srinivas, S., Vijayalakshmi, A., Reddy, A. S., Ramamohan, T.R (2016). MHD flow of a nanofluid in an expanding or contracting porous pipe with chemical reaction and heat source/ sink, *Propulsion and Power Research*, 5(2):134–148.